On the system performance of DFT-S-OFDM and CP-OFDM for 5G Uplink in mmWave band

Alejandro Villena-Rodríguez[(1)], Francisco J. Martín-Vega[(1)], F. Javier López-Martínez[(1)], Gerardo Gómez[(1)]
José Outes-Carnero[(2)], F. Yak Ng-Molina [(2)], Juan Ramiro-Moreno[(2)]
{avr, fjmvega, fjlopezm, ggomez}@ic.uma.es, {jose.outes, yak.ng.molina, juan.ramiro}@ericsson.com
[(1)]Dpto. Ingeniería de Comunicaciones. Universidad de Málaga. ETSI Telecomunicación, 29071.
[(2)] Ericsson, Málaga, Spain.

***Abstract*—Both conventional Cyclic Prefix Orthogonal Frequency Division Multiplexing (CP-OFDM) and Discrete Fourier Transform Spread OFDM (DFT-S-OFDM) have been adopted for their use in the Physical Uplink Shared Channel (PUSCH) in the 5G New Radio (NR) standard. While CP-OFDM can better exploit the frequency characteristics of the channel, DFT-S-OFDM has the advantage of a lower peak-to-average power ratio (PAPR). Due to the interactions between PAPR and power amplifier (PA) non-linearity, users adopting DFT-S-OFDM waveform may benefit from a potentially higher PA efficiency and extend their coverage by increasing their transmit power. In this paper we study the uplink performance of both waveforms and their interaction with non-linear PA and uplink power control in the millimeter-wave (mmWave) band to determine their optimal operational range.**

I. Introduction

One of the key challenges of next-generation mobile networks is to support a wide range of applications and deployment scenarios. For that purpose, the 5G standard provides a set of flexible features that allow an efficient use of the radio resources, being one of the most important features the use of different waveforms. For the uplink (UL), two different waveforms are considered by 3GPP [1], namely the conventional Cyclic Prefix-Orthogonal Frequency Division Multiplexing (CP-OFDM) and Discrete Fourier Transform Spread OFDM (DFT-S-OFDM); each one of them can be selected depending on different channel conditions and deployment scenarios.

CP-OFDM has been broadly studied and commercially implemented due to the simplicity of the receiver architecture and its high spectral efficiency. However, it suffers from a high peak-to-average power ratio (PAPR), a characteristic that its counterpart DFT-S-OFDM does not share. The low PAPR in DFT-S-OFDM benefits the user equipment (UE) power consumption, power amplifier (PA) efficiency and manufacturing costs, and allows to increase its coverage range [2]. In addition, a lower PAPR leads to a weaker interaction with the non-linearities of the PA. Previous works [3] have shown that in presence of a non-linear PA and UL power control, DFT-S-OFDM leads to lower errors and a higher throughput compared to CP-OFDM, whenever the UE is far enough from the base station. These studies have been focused on LTE, although to the best of the authors' knowledge, the impact of the different waveforms on a mmWave channel for 5G scenarios has not been addressed yet.

In this paper we compare the performance of DFT-S-OFDM and CP-OFDM under a mmWave channel for a typical 5G physical layer configuration, focusing on the impact of UL power control and PA non-linearities.

The rest of the paper is organized as follows. Section II summarizes the system model. Simulation results are discussed in Section III. Finally, section IV draws the main conclusions of this work.

II. System Overview

For exemplary purposes, a single-cell single-user system in the UL direction is studied. The proposed system considers two different UL access schemes:

- DFT-S-OFDM waveform with 1 antenna port and 1 data layer,
- CP-OFDM waveform with 2 antenna ports and 1 data layer.

To simulate a realistic scenario, the time-domain signals generated by each access scheme, which are detailed in subsections II-A and II-B, are amplified by a non-linear PA as described in subsection II-C where the working output power of the PA is dictated by the UL Power Control explained in subsection II-D. At the end of this section it is also included the Signal to Noise Ratio definition considered in this work in subsection II-E. It is worth noting that the DFT-S-OFDM system only makes use of 1 antenna port. This design decision was taken due to the moderate to low compatibility with multiple-input multiple-output (MIMO) [4].

A. CP-OFDM Signal Generation

Let the elements of vector $\mathbf{d} \in \mathbb{C}^{1\times N_d}$ be a set of data symbols to be transmitted, being N_d the number of data symbols. Symbols are transformed via a precoding matrix $\mathbf{W} \in \mathbb{C}^{N_{\text{tx}}\times 1}$ where N_{tx} is the number of antenna ports. This precoding matrix maps data layers onto the number of antenna ports. For simplicity, the precoding matrix considered in this paper is built for 1 data layer and 2 antenna ports as $\mathbf{W} = [1 \quad 1]^T/\sqrt{2}$. After the multiplication with the matrix $\mathbf{W}$, the resulting data symbols are transposed. Then, the precoded and transposed symbols are mapped onto the input of the IDFT via a mapping matrix $\mathbf{T} \in \mathbb{C}^{N\times N_d}$, where N is the number of subcarriers. Finally, the output of the matrix $\mathbf{T}$ is converted to the time domain via $\mathbf{F}^H$ where $\mathbf{F}^H \in \mathbb{C}^{N\times N}$ is the inverse DFT (IDFT). The final signal $\mathbf{x} \in \mathbb{C}^{N\times N_{\text{tx}}}$ in the time domain is generated as following:

$$\mathbf{x} = \mathbf{F^H T (Wd)^T}. \tag{1}$$

Afterwards, a cyclic prefix is added to the resulting time signal before being fed into the non-linear PA. Fig. 1 shows the CP-OFDM signal generation process from eq. (1).

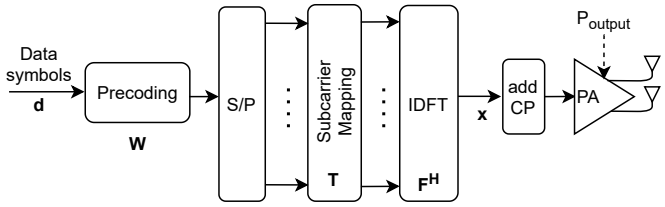

Fig. 1. Digital base-band transmitter structure of CP-OFDM

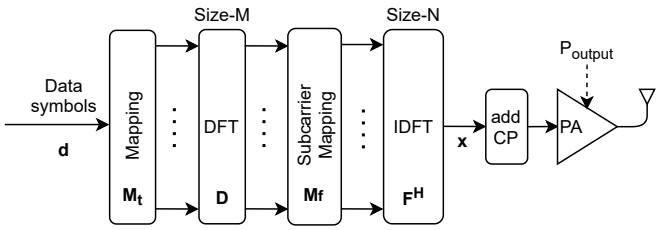

Fig. 2. Digital base-band transmitter structure of DFT-S-OFDM

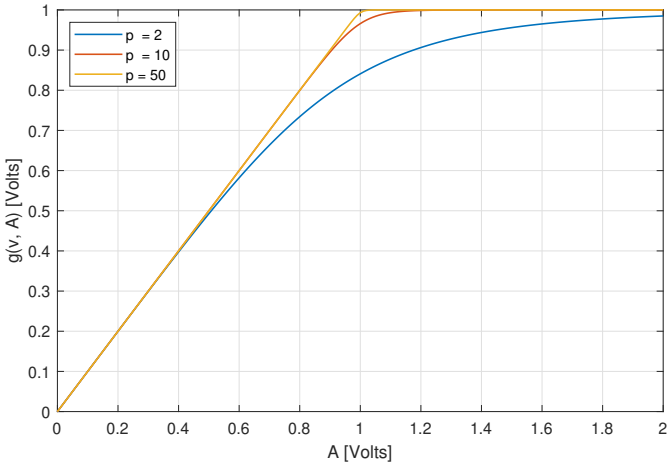

Fig. 3. Rapp model of PA AM/AM non-linearity, with $A = A_{\text{sat}} = 1$ volts.

B. DFT-S-OFDM Signal Generation

Let the elements of vector $\mathbf{d} \in \mathbb{C}^{N_d \times 1}$ be a set of data symbols to be transmitted, being N_d the number of data symbols. Data symbols are mapped onto the input of a DFT matrix denoted by $\mathbf{D} \in \mathbb{C}^{M \times M}$ via a mapping matrix $\mathbf{M_t} \in \mathbb{C}^{M \times N_d}$ where M is the DFT size. Then, the output of the DFT is mapped onto a set of subcarriers in the frequency domain through another mapping matrix $\mathbf{M_f} \in \mathbb{C}^{N \times M}$. Finally, the output of the matrix $\mathbf{M_f}$ is converted to time domain via $\mathbf{F}^H$ where $\mathbf{F}^H \in \mathbb{C}^{N \times N}$ is the inverse DFT (IDFT) matrix and N is the number of subcarriers. The final signal $\mathbf{x} \in \mathbb{C}^{N \times 1}$ in the time domain is generated as follows:

$$\mathbf{x} = \mathbf{F}^H \mathbf{M_f} \mathbf{D_t} \mathbf{M_t} \mathbf{d}. \tag{2}$$

Afterwards, a cyclic prefix is added to the resulting time signal before being fed into the non-linear PA. Fig. 2 shows the DFT-S-OFDM signal generation process from eq. (2).

C. Non-linearity of Power Amplifiers

For the sake of simplicity, the PA is assumed to be memory-less with amplitude-to-amplitude (AM/AM) distortion only. More precisely, the PA model implemented in this paper is the Rapp model of a typical solid state high power amplifier (SSPA) described in [5] and which amplitude-to-amplitude conversion function is given by:

$$g(v, A) = v \frac{A}{\left(1 + \text{abs}\left(\frac{vA}{A_{\text{sat}}}\right)^{2p}\right)^{\frac{1}{2p}}}, \tag{3}$$

where v is the small signal gain, A is the amplitude of the input signal, A_{sat} is the limiting output amplitude and p controls the smoothness of the transition from the linear region to the saturation regime. Fig. 3 shows the amplitude transfer function from eq. (3) for different values of p.

D. Uplink Power Control

Power control is of paramount importance in the UL of 5G NR since it aims at guaranteeing a target received power at the BS, P_0, while minimizing the transmitted power in order to save battery and reduce interference leaked towards neighbouring cells. To this end, the UEs adjust their transmit power so as to compensate the pathloss and shadowing. For this reason, UL power control is especially relevant at higher frequency bands where the pathloss is higher than in lower bands, as those used on previous 4G standards. We have considered the closed-loop UL power control of the Physical Uplink Shared Channel (PUSCH) as studied in [6]. This method considers that the UE and BS decide a transmit power, P_{decided}, to compensate for the pathloss, PL. This decided transmit power is based on the sum of two parts: An open power control part, that the UE computes based on DL reference signals; and an offset that is based on Transmit Power Control (TPC) commands received from the BS on the UL grant assignments. After a number of TPC receptions, the decided transmit power converges to the following value:

$$P_{\text{decided}} = P_0 + \alpha \times \text{PL} \quad [\text{dBW}], \tag{4}$$

where PL is the pathloss, which is drawn from the Urban Macro (UMa) distribution in [7], and $\alpha \in [0, 1]$ is the fractional compensation factor. This latter parameter allows to get a balance between desired received power at the serving BS and interference generated towards neighbouring cells [8], [9]. If $\alpha = 0$, the pathloss is not compensated, and thus $P_{\text{decided}} = P_0$, whereas with $\alpha = 1$, P_{decided} fully compensates the pathloss. As shown in [8], values close to $\alpha = 0.75$ maximizes average capacity when the BSs are placed randomly according to a Poisson point process. Restrictions on the maximum transmit power supported by the UE and also out-of-band emissions, impose further limits on the transmitted power. Thus, the final power transmitted by the UE, P_{output}, can be defined as:

$$P_{\text{output}} = \min(P_{\text{decided}}, P'_{\text{max}}) \ [\text{dBW}], \tag{5}$$

where $P'_{\text{max}} = P_{\text{max}} - \text{MPR}$ [dBW]. The Maximum Power Reduction (MPR) [10] specifies the decrease in the maximum power transmitted in order to enable the device to fulfil the requirements of the transmitter adjacent channel leakage ratio. This value imposes a maximum transmit power to guarantee that the out-of-band emission is below a given threshold. Since, this out-of-band emissions depend on the waveform, modulation level and channel bandwidth, the possible values

TABLE I
MPR (DB) VALUES

Waveform	Modulation	MPR (dB) 50/100/200 MHz Channel BW	MPR (dB) 400 MHz Channel BW
DFT-S-OFDM	Pi/2BPSK	1.5	3.0
	QPSK	1.5	3.0
	16QAM	3.0	4.5
	64QAM	5.0	6.5
CP-OFDM	QPSK	3.5	5.0
	16QAM	5.0	6.5
	64QAM	7.5	9.0

of MPR also depends on such parameters. Table I summarizes the power reduction values. Notice that a higher maximum power can be used with DFT-S-OFDM, since its MPR is smaller than with CP-OFDM. This is an expected result as the former waveform is related to a smaller PAPR. DFT-S-OFDM has shown PAPR values between 7 and 8.5 dB while CP-OFDM produced values between 10 and 11 dB.

E. Signal to Noise Ratio metric

The Signal to Noise Ratio (SNR) definition considered in this paper is given by the following expression:

$$\text{SNR} = P_{\text{output}} - PL + 10\log_{10}(\sum_{i=1}^{N_{rx}} |h_i|^2) - N_0 \quad [\text{dB}] \quad (6)$$

where P_{output} is the UE output power from eq. (5), PL is the estimated pathloss, N_{rx} is the number of receiver antennas, h_i is the effective channel of the i-th receiver antenna after channel estimation and N_0 is the thermal noise in the band assigned to the user, given by

$$N_0 = -204 + 10\log_{10}(12 \times \Delta f \times N_{RB}) + N_{\text{fig}} \quad [\text{dBW}] \quad (7)$$

where Δf is the subcarrier spacing in Hz, N_{RB} is the number of Physical Resource Blocks (PRBs) assigned to the user and N_{fig} is the noise figure at the BS in dB.

III. SIMULATION RESULTS

The impact of the UL power control and the PA non-linearities on the performance for each transmission scheme is evaluated in this section. The key simulation parameters are summarized in Table II.

Fig. 4 shows the differences in average received SNR for the waveforms under study. Due to pathloss and output power restrictions, the SNR values decay with the distance once P_{decided} is equal or higher than P'_{max}. From that point on, the UE starts transmitting with the highest possible output power, P'_{max}. Fig. 4 confirms that the SNR of the DFT-S-OFDM case is larger than that of the CP-OFDM case. This is mainly due to eq. (5) and the fact that MPR values in Table I take larger values for the CP-OFDM case. Therefore, higher output powers are used for the DFT-S-OFDM waveform, leading to higher SNRs given the same noise level for both waveforms.

Fig. 5 illustrates Bit Error Rate (BER) results for both waveforms as a function of the distance to the BS. For shorter distances, CP-OFDM waveform with 2 antenna ports has a

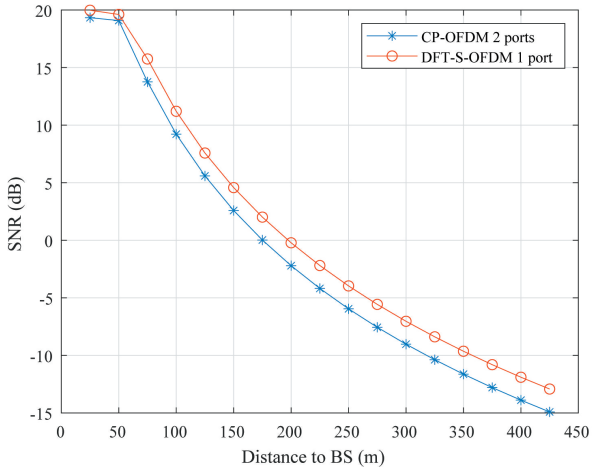

Fig. 4. Average received SNR vs. distance to the BS, for both waveforms.

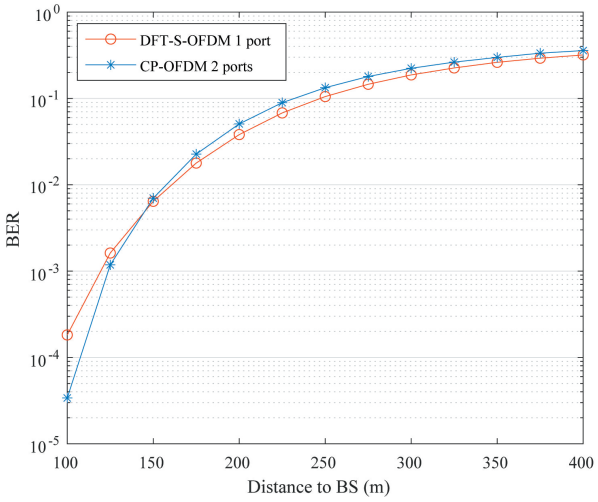

Fig. 5. BER vs SNR for both waveforms.

better error performance than DFT-S-OFDM waveform with 1 antenna port. At around 150 meters, there is a cross-point and, above that distance, simulations show a change in the behaviour of the BER results. We see that DFT-S-OFDM waveform with 1 antenna port is now the transmission scheme with a lower BER. This change in behaviour is also present when we study the Block Error Rate (BLER) in the same scenario, as shown in Fig. 6. This suggests that switching from a 2-port CP-OFDM mode to a 1-port DFT-S-OFDM operation is beneficial for users close to the cell edge.

Fig. 7 shows the goodput of both waveforms against the received SNR. For each simulation point, the goodput metric, which indicates the amount of error-free data compared to the total amount of information transmitted, is defined by:

$$\text{Goodput} = \frac{Throughput \times (1 - \text{BLER})}{Throughput_{max}} \times 100 \quad (\%) \quad (8)$$

where $Throughput$ is the amount of data transmitted for that simulation point and $Throughput_{max}$ is the maximum amount of data transmitted for each waveform. For SNR values under -2dB approximately, DFT-S-OFDM waveform

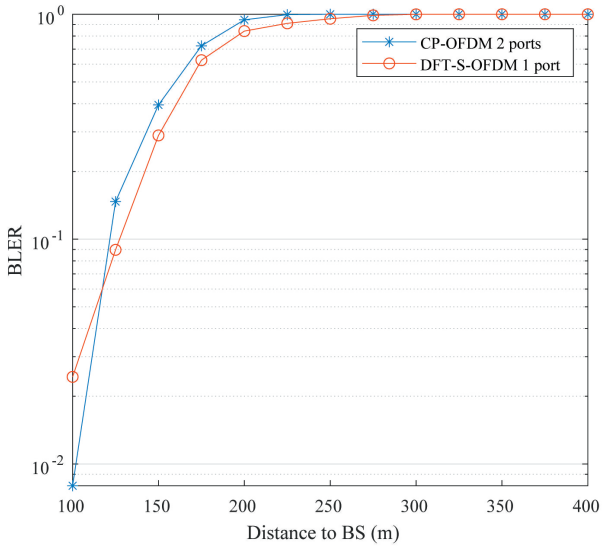

Fig. 6. BLER vs SNR for both waveforms.

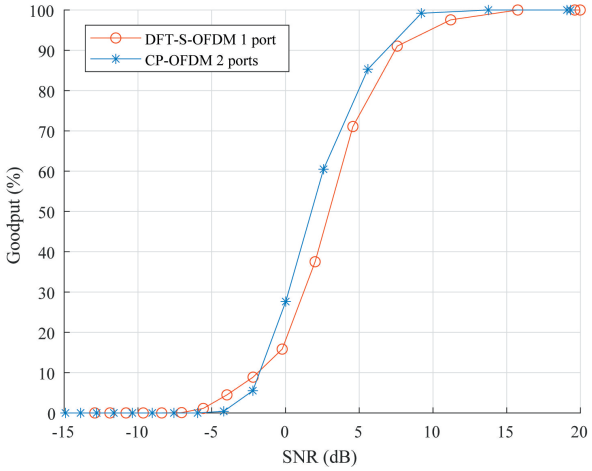

Fig. 7. Goodput vs SNR for both waveforms.

with 1 antenna port achieves the highest goodput. However, it remains worse in terms of goodput from the -2dB cross-point until SNR values above 15dB, where both waveforms reach the 100% goodput.

IV. Conclusions

We compared the performance of CP-OFDM with 2 antenna ports and DFT-S-OFDM with 1 antenna port, in a realistic set-up that considers the effects of non-linear amplifiers and UL power control in a 5G simulation scenario for the mmWave band. Even though CP-OFDM presents many major advantages, such as reliability in multipath transmissions, compatibility with MIMO systems and a relative insensitivity to timing offset [11], it is shown that DFT-S-OFDM is more robust and brings a better performance when the UE faces lower SNR scenarios at the cell edge. This is due to its lower sensitivity to the PA non-linearity and the difference in MPR values, leading to a higher output power. According to these results, an interesting feature to improve the overall performance would be to define a dynamic switching method between the two transmission schemes. Nonetheless, we found that the cross-point in the performance is observed to have a high dependence on several parameters such as bandwidth, MCS mode, PA characteristics and subcarrier spacing, among others, making necessary further exploration of the issue.

TABLE II
Simulation Parameters

Channel model	CDL-A
Pathloss model	UMa
α in UL power control	1
UE $P_{\max}$	24 dBm
Carrier frequency	28 GHz
Subcarrier spacing	15 kHz
Number of PRBs per user	4
BS bandwidth (PRB)	270
p in Rapp model	2
Noise figure	2 dB
MCS	2
Channel estimation	Least Squares (LS)

Acknowledgements

This work has been funded by the European Fund for Regional Development (FEDER) and Junta de Andalucía under the projects P18-RT-3175, P18-TP-3587, UMA-CEIATECH-06 and PAIDI 2020, the University of Málaga and Ericsson, who has submitted application no. 702C2000043 for funding called by Junta de Andalucía.

References

[1] 3GPP TS 38.211 V15.5.0. "In Technical Specification Group Radio Access Network; Physical Channels and Modulation (Release 15)". April, 2019.
[2] Sahin, A., Yang, R., Bala, E., Beluri, M. C., & Olesen, R. L. (2016). Flexible DFT-S-OFDM: solutions and challenges. IEEE Communications Magazine, 54(11), 106-112.
[3] Zheng, K., Wei, M., Long, H., Liu, Y., ans Wang, W. "Impacts of amplifier non-linearities on uplink performance in 3G LTE systems." in 2009 Fourth International Conference on Communications and Networking in China. IEEE, August 2009, pp. 1 - 5.
[4] Zaidi, A. A., Luo, J., Gerzaguet, R., Wolfgang, A., Weiler, R. J., Vihriälä, J., ... & Miao, H. "A preliminary study on waveform candidates for 5G mobile radio communications above 6 GHz". In 2016 IEEE 83rd Vehicular Technology Conference (VTC Spring) (pp. 1-6). IEEE. May, 2016. pp. 1 - 6.
[5] RAPP, Christoph. "Effects of HPA-non-linearity on a 4-DPSK/OFDM-signal for a digital sound broadcasting signal". ESA Special Publication, 1991, vol. 332, p. 179-184.
[6] Simonsson, A., & Furuskar, A.. "Uplink power control in LTE-overview and performance, subtitle: principles and benefits of utilizing rather than compensating for SINR variations". In 2008 IEEE 68th Vehicular Technology Conference. IEEE. September, 2008. pp. 1 - 5.
[7] 3GPP TR 38.901 v15.0.0. "Study on channel model for frequencies from 0.5 to 100 GHz (Release 15)". July, 2018
[8] F. J. Martin-Vega, G. Gomez, M. C. Aguayo-Torres and M. Di Renzo, "Analytical Modeling of Interference Aware Power Control for the Uplink of Heterogeneous Cellular Networks," in IEEE Transactions on Wireless Communications, vol. 15, no. 10, pp. 6742-6757, October 2016.
[9] Martín-Vega, F. J., Xi, X., Di Renzo, M. et al. "On muting mobile terminals for uplink interference mitigation in HetNets—system-level analysis via stochastic geometry". J Wireless Com Network 2019, 100 (2019).
[10] 3GPP TS 38.101-2 v15.3.0, "User Equipment (UE) radio transmission and reception ; Part 2: Range 2 Standalone (Release 15)". October 2018.
[11] Kongara, G., He, C., Yang, L., & Armstrong, J. (2019). "A comparison of CP-OFDM, PCC-OFDM and UFMC for 5G uplink communications. IEEE Access, 7, 157574-157594.